# Investigations on low temperature laser-generated plasmas

F. CARIDI, L. TORRISI, D. MARGARONE, AND A. BORRIELLI

Dipartimento di Fisica, Messina, Italy and INFN-LNS and INFN Sezione di Catania (Gr. Coll. Messina), Catania, Italy

(RECEIVED 18 December 2007; ACCEPTED 25 March 2008)

**Abstract**

A nanosecond pulsed Nd-Yag laser, operating at an intensity of about $10^9$ W/cm$^2$, was employed to irradiate different metallic solid targets (Al, Cu, Ta, W, and Au) in vacuum. The measured ablation yield increases with the direct current (dc) electrical conductivity of the irradiated target. The produced plasma was characterized in terms of thermal and Coulomb interaction evaluating the ion temperature and the ion acceleration voltage developed in the non-equilibrium plasma core. The particles emission produced along the normal to the target surface was investigated measuring the neutral and the ion energy distributions and fitting the experimental data with the "Coulomb-Boltzmann-shifted" function. Results indicate that the mean energy of the distributions and the equivalent ion acceleration voltage of the non-equilibrium plasma increase with the free electron density of the irradiated element.

**Keywords:** Electron density; Ion energy distribution; Laser-generated plasma

## INTRODUCTION

Pulsed lasers with nanosecond pulse duration and intensities on the order of $10^{10}$ W/cm$^2$ are largely employed in different fields, from microelectronics to laser ion sources, from cultural heritage to biomedical applications (Batani *et al.*, 2007; Jungwirth 2005; Schaumann *et al.*, 2005; Veiko *et al.*, 2006). The laser-generated plasma, in fact, can be used to imprint surfaces, to generate ions at high energy and charge state, to clean the surface of old coins, and to deposit biocompatible thin films on medical prosthesis by means of the pulsed laser deposition technique (Bashir *et al.*, 2007; Conde *et al.*, 2004; Fernandez *et al.*, 2005; Lorazo *et al.*, 2006; Nelea *et al.*, 2004; Thareja & Sharma 2006; Wieger *et al.*, 2006; Wolowski *et al.*, 2007).

Although many applications of these lasers exist at present, further investigations are necessary in order to characterize the laser-produced plasmas in terms of ion and electron temperature, density, fractional ionization, angular distribution, and dependence of the plasma parameters on the nature of the laser irradiated target.

The electron density of the plasma, in fact, determines the plasma evolution kinetics, the inverse bremsstrahlung laser absorption, the electron-ion interaction and ionization processes, the recombination and the charge separation effects which produce, in times on the order of a few nanoseconds, a high electric field inside the plasma. This field is responsible for the ion acceleration and for the ion energy distributions separation as a function of the charge state (Laska *et al.*, 2007; Torrisi *et al.*, 2006). The thermal processes occurring in the Knudsen layer, close to the target surface, can be understood evaluating the plasma temperature by assuming that the ionized gas is in a local thermal equilibrium (LTE) condition. The temperature can be measured directly knowing the energy distribution of the neutral species emitted from the plasma or with other methods.

For infrared and visible laser irradiation, the free electron density of the target element and its dc electrical conductivity, $\sigma_{dc}$, are important parameters that determine the final properties of the produced plasma, such as ablation yield, temperature, and electric field developed inside it.

In this work, in order to measure the energy distributions for the various charge states and to evaluate their dependence on the free electron density of the irradiated elements, measurements were performed with a mass quadrupole spectrometer with electrostatic deflection. The free electrons of metallic targets are the first cause of infrared and visible laser light absorption in the material, determining the laser penetration depth, the thermal conductivity, the target reflectivity and, as it will be demonstrated, the equivalent ion temperature of the developed non-equilibrium plasma.

Address correspondence and reprint requests to: Francesco Caridi, Dipartimento di Fisica, Ctr. Papardo 31, 98166 S. Agata, Messina, Italy. E-mail: fcaridi@unime.it

## MATERIALS AND METHODS

The nanosecond ablation experiments have employed a Nd:Yag laser operating at 532 nm (second harmonic) at the Messina University laboratory, with 3 ns pulse duration, in single pulse or at 10 Hz repetition rate, with a maximum pulse energy of 150 mJ. Measurements were made at 25 mJ, to minimize the crater effects, focusing the laser beam on the target surface with a spot size of about 0.5 mm$^2$ at 45° incidence angle. The corresponding laser intensity was $1.7 \times 10^9$ W/cm$^2$.

The experimental setup comprises a high vacuum chamber, a central rotating target holder, which permits vertical movement of the target to change the spot position and to rotate the target to change the incidence angle, and an electrostatic mass quadrupole analyzer placed at 45° with respect to the laser beam direction and at 0° with respect to the normal to the target surface. A schematic overview of the set up is shown in Figure 1a.

The pressure in the chamber was maintained at about $2 \times 10^{-6}$ mbar. The targets used in this investigation were $2 \times 2$ cm surface and 1 mm thickness pure Al, Cu, Ta, W, and Au.
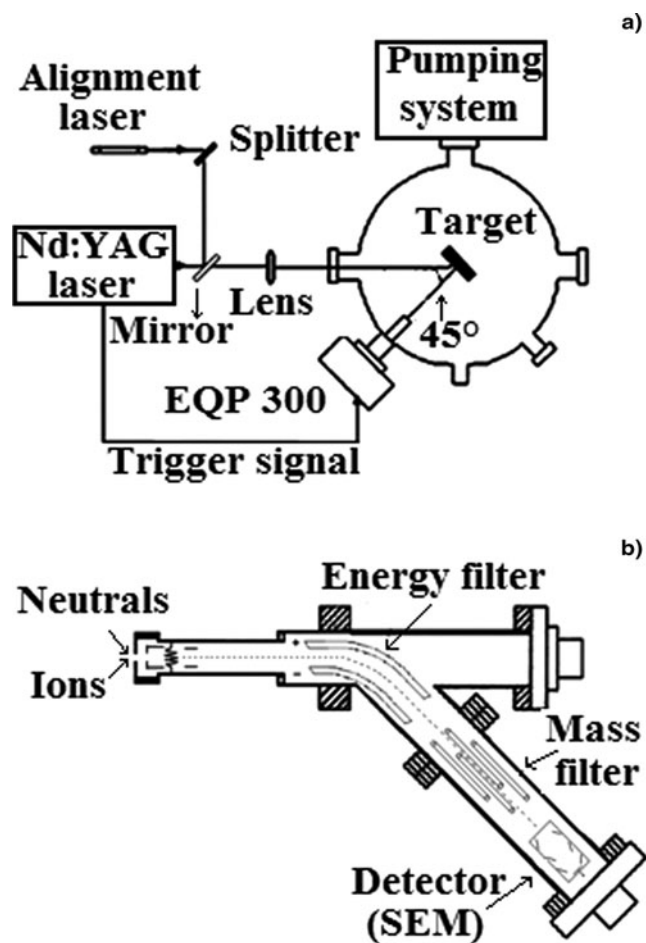
A special electrostatic mass quadrupole spectrometer, the so-called Electrostatic Quadrupole Plasma (EQP Hiden 300), was employed to monitor the particles ejected from the plasma with a mass range within 1 and 300 amu. The instrument detects neutrals and charged particles depending on the filament state (with filament "on" neutrals and ions are both detected while with filament "off" only ions are detected). The charge state is monitored through the mass-to-charge ratio measurement performed by an electrostatic ion deflection. It measures the particle energy with an accuracy of $\pm 5$ eV and plots the energy distribution of neutral and charged species in the energy range 1 eV – 1 keV.

Figure 1b shows the scheme of the EQP instrument. The spectra acquisition occurs operating at 10 Hz laser repetition rate, and it is triggered with the laser shot. A full EQP analysis employs about 1 – 2 min, during which 600 or 1200 laser shots irradiate the target. EQP uses a 45° electrostatic deflection, in order to measure the ion energy, and a differential pumping at $1 \times 10^{-7}$ mbar pressure. The instrument consists of four main sections: the ionisation source; the electrostatic energy filter; the mass filter; the secondary electron multiplier (SEM) detector. More details on the EQP instrument are reported in the literature (Hiden Analytical website 2006).

EQP spectra were analysed in order to separate the neutral component from the ionic one and to plot the particle energy distributions for the various charge states. The fits of the experimental energy distributions were performed with the "Coulomb-Boltzmann-shifted" function used in previous works (Torrisi *et al.*, 2002) through the "Peakfit" numerical code (Cranes software website 2006).

The ablation yield was measured calculating the number of removed atoms per laser pulse from the laser-generated crater on the target. The crater profiles were investigated with optical microscopy and surface profiler (Tencor-P10), which depth and lateral resolution was about 10 nm.

## RESULTS AND DISCUSSION

Figure 2a shows a comparison of the crater profiles obtained irradiating the five elements (Al, Cu, Ta, W, and Au ) in the same experimental conditions, at 0° incidence angle. It is possible to observe that the crater volume decreases from Al to Ta. The ablated mass per laser pulse can be calculated through the crater volume and the target density, giving a maximum value of 0.24 µg/pulse for Au and a minimum value of 0.03 µg/pulse for Al. The ablation yield, expressed in terms of removed atoms per laser pulse, gives a maximum value for Cu ($12 \times 10^{14}$ atoms/pulse) and a minimum value for Ta ($4 \times 10^{14}$ atoms/pulse). Obtained results indicate that the ablation yield increases linearly with the dc electrical conductivity of the target, as reported in Figure 2b.

Figure 3 shows two typical EQP spectra obtained ablating Cu and W targets at 25 mJ pulse energy and 10 Hz
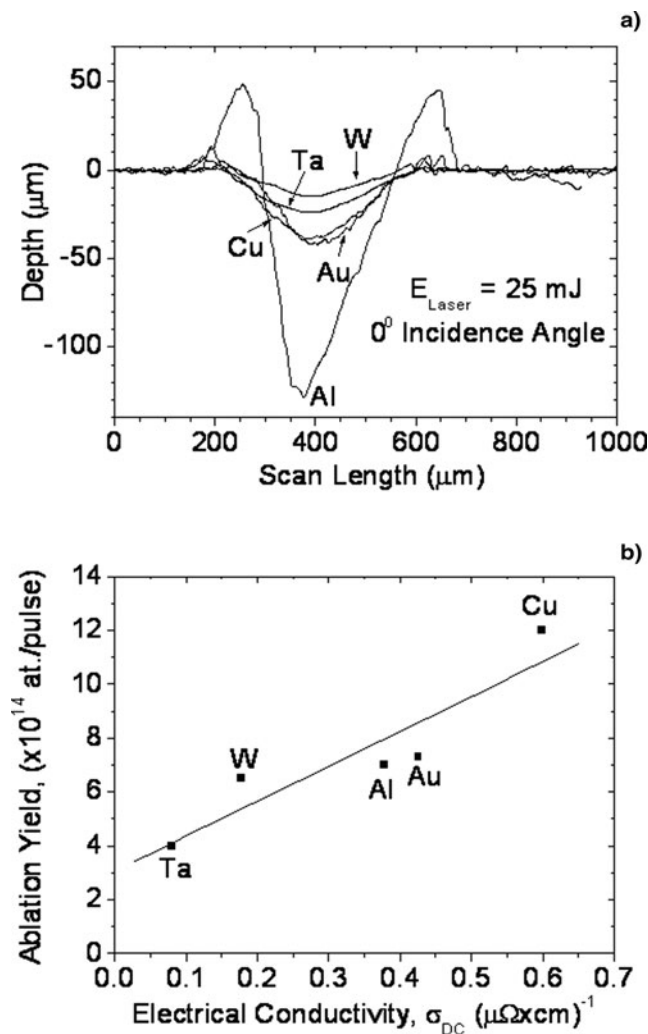


**Fig. 1.** The experimental setup (**a**) and the scheme of the EQP instrument (**b**).

Fig. 2. Crater profiles comparison (**a**) and ablation yield versus dc electrical conductivity (**b**).





**Fig. 3.** Two typical EQP spectra obtained ablating Cu (**a**) and W (**b**) targets at 25 mJ pulse energy and 10 Hz repetition rate.

repetition rate. Spectra report the yield signal versus particle energy for neutrals and for single and double ionized atoms. The fit of the experimental data (vertical bars) indicates that the particles have typical Boltzmann distributions peaked at different energies depending on their charge state. In particular, neutrals are peaked at energies of about 15 eV and 25 eV for Cu and W, respectively, while the first ionized atoms are peaked at about 62 eV and 85 eV in the two cases. The second ionized atoms are peaked at a higher energy, of about 110 V and 150 eV, respectively.

Neutrals energy distributions contain direct information on the plasma temperature. Along the normal to the target irradiation this energy is due to two different contributions: the first is due to the thermal energy, $E_T = 3kT/2$ and the second to the adiabatic expansion energy, $E_K = \gamma kT/2$, where $k$ is the Boltzmann constant, $T$ is the temperature, and $\gamma$ is the adiabatic coefficient ($1.67 = 5/3$ for monoatomic species).
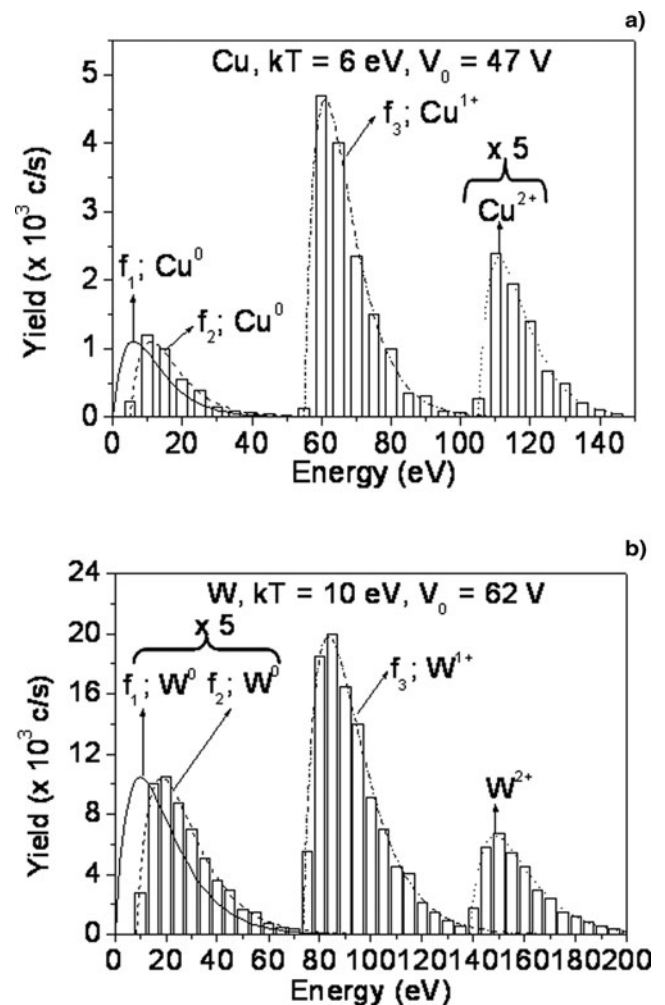
Thus the neutrals energy distribution doesn't follow a simple Boltzmann function:

$$f_1 = \frac{A_1}{2}\sqrt{\frac{2}{m}}\sqrt{\frac{1}{(\pi kT)^3}}E \exp\left(-\frac{E}{kT}\right) \qquad (1)$$

but it must be written as a Boltzmann shifted function (Torrisi *et al.*, 2002):

$$f_2 = \frac{A_1}{2}\sqrt{\frac{2}{m}}\sqrt{\frac{1}{(\pi kT)^3}}(E - E_K) \exp\left(-\frac{E - E_K}{kT}\right) \qquad (2)$$

where $A_1$ represents the normalization constant, $m$ is the atomic mass, and $E$ is the total energy of the neutrals along the normal to the target surface.

The fit of experimental spectra with Eq. (2) indicates that the temperature for Cu and W plasmas is 6 eV and 10 eV, respectively. The ion energy distributions contain information not only about the temperature but also about the

Coulomb interactions. In this case, in fact, a third contribution is involved in the total ion energy; this is the Coulomb energy, $E_C = zeV_0$, where $ze$ is the ion charge and $V_0$ is the acceleration voltage developed inside the non-equilibrium plasma. As previously reported in literature, in this case, the experimental data follow a Coulomb-Boltzmann-shifted distribution (Torrisi *et al.*, 2002):

$$f_3 = \frac{A_3}{2}\sqrt{\frac{2}{m}}\sqrt{\frac{1}{(\pi kT)^3}}(E - E_K - E_C)\exp\left(-\frac{E - E_K - E_C}{kT}\right) \quad (3)$$

Data regarding the first ionized atoms can be fitted by Eq. (3) assuming the temperature $kT$ to be 6 eV and 10 eV and the acceleration voltage $V_0$ about 47 V and 62 V for Cu and W, respectively.

The different results obtained irradiating Cu and W targets under the same experimental conditions can be explained on the basis of the different physical properties of the two elements. One of these properties is represented by the number of free electrons of conduction in metals, which are weakly bounded to the elemental atom. In fact, for elements characterized by an high electron density value, there will be a higher amount of electrons in the dense vapor, immediately after the laser ablation. These electrons absorb the laser photons energy through the inverse bremsstrahlung process reaching energies suitable to induce ionization processes. Also data regarding the second ionized atoms can be fitted by Eq. (3) with a suitable value of the $A$ normalization constant. This fit leads back to the plasma temperature $kT$ and to the acceleration voltage $V_0$, which is in agreement with the data obtained analyzing the single ionized atoms energy distributions.

The analysis of the EQP spectra for the five irradiated targets allows us to study the dependence of the particles yield and energy on the physical properties of the irradiated target. For elements with a low value of the ablation threshold, calculated through the approach given by Torrisi *et al.* (2007), with a low thermal conductivity, as Al for example, only a small fraction of the laser pulse energy is used for the evaporation. As a consequence, above the threshold the ablation yield is generally high ($7 \times 10^{14}$ atoms/pulse for Al at 25 mJ laser pulse), because of the remaining high laser pulse energy transferred to the

plasma. On the contrary, for elements with an higher value of the ablation threshold, as W for example, a higher amount of the laser pulse energy is necessary to produce its evaporation in vacuum, and the ablation yield is lower ($6.5 \times 10^{14}$ atoms/pulse for W at 25 mJ laser pulse) as a consequence of the remaining low pulse energy transferred to the plasma.

Moreover, we expect that the mean energy transferred by the laser pulse to the atoms of the vapor is low when the target has a low evaporation point and high ablation yield, as Cu for example, because many atoms compose a dense vapor (Torrisi *et al.*, 2003). On the contrary, the mean energy is high when the target has a high evaporation point and low ablation yield, as W for example, because the vapor is less dense. This is in good agreement with our experimental results detailed in Table 1.

Measurements demonstrated that the neutrals peak energy grows with the free electron density of the irradiated targets, as reported in Figure 4a. The free electron density was calculated multiplying the atomic density of the element for its electron valence. The used values of electron densities are reported in the first column of Table 1 for the five irradiated metals.

The corresponding temperature of the produced plasma, obtained as fit parameter of Eq. (2), increases linearly with the electron density of the element, as reported in Figure 4b. Thus, the free electron density in the irradiated metal seems to be a good parameter which characterizes the plasma properties, probably because it is linked to the inverse bremsstrahlung absorption mechanism. Targets with high free electron density absorb more energy from the laser beam, with respect to those with low free electron density, and their energy transfer to the atoms of the vapour increases the plasma temperature.

The analysis of the EQP spectra have also allows us to study the dependence of the ions 1+ energy distributions on the physical nature of the irradiated target. Measurements demonstrated that the peak energy of the first ionized atoms grows with the free electron density of the irradiated target, as reported in Figure 5a. This result confirms that the energy transferred is proportional to this important physical parameter of the ablated element. In the case of the ion energy distribution, the evaluation of the energy shifts with respect to the neutrals distribution allows us to calculate the ion equivalent

**Table 1.** *The main parameters characterizing the five laser-generated plasmas*

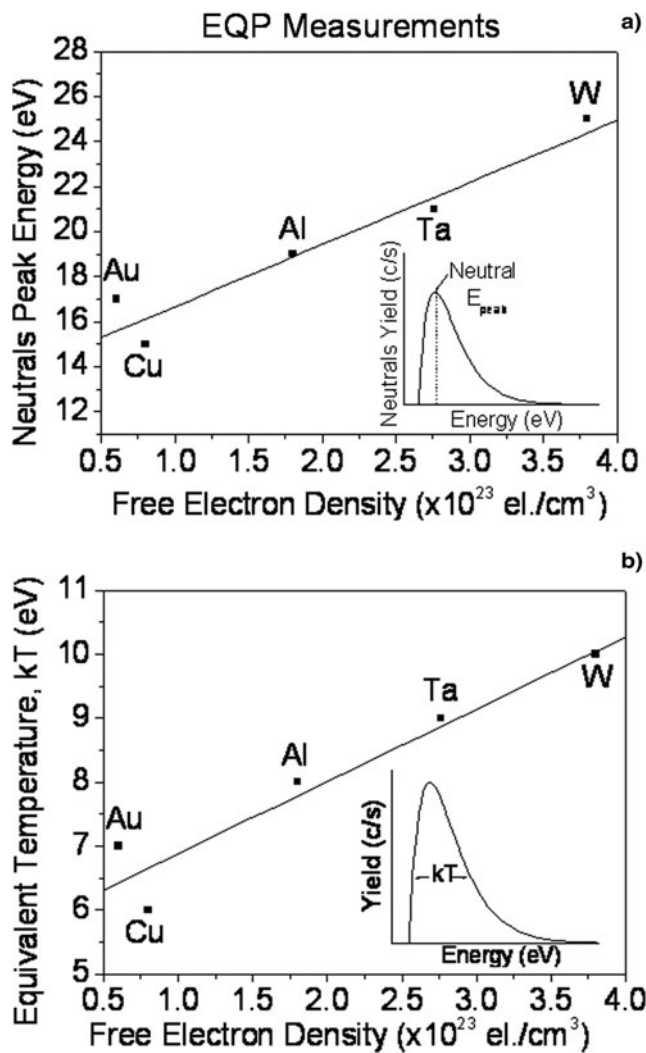| El. | Free electron density ($\times 10^{23}$/cm$^3$) | Theorical ablation threshold (J/cm$^2$) | Removed mass (µg/p) | Ablation yield ($\times 10^{14}$ ats/p) | $E_n$ (eV) | $E_{1+}$ (eV) | $E_{2+}$ (eV) | $Y^{1+}/Y^0$ | $Y^{1+}/Y^{2+}$ | $V_0$ (V) | $kT$ (eV) |
|---|---|---|---|---|---|---|---|---|---|---|---|
| Cu | 0.8 | 1.04 | 0.13 | 12 | 15 | 62 | 110 | 1.5 | 3.6 | 47 | 6 |
| Au | 0.6 | 0.8 | 0.24 | 7.3 | 17 | 67 | 116 | 1.8 | 3.5 | 49 | 7 |
| Al | 1.8 | 0.6 | 0.03 | 7 | 19 | 72 | 125 | 3.7 | 3.3 | 53 | 8 |
| Ta | 2.7 | 0.7 | 0.12 | 4 | 21 | 79 | 137 | 6.5 | 3.1 | 58 | 9 |
| W | 3.8 | 1.3 | 0.2 | 6.5 | 25 | 85 | 150 | 8.9 | 2.8 | 62 | 10 |

**Fig. 4.** The neutrals peak energy (**a**) and the corresponding temperature of the produced plasma (**b**) as a function of the free electron density of the irradiated targets.



**Fig. 5.** The ions 1+ peak energy (**a**) and the equivalent acceleration voltage (**b**) as a function of the free electron density of the ablated elements.

acceleration voltage $V_0$, in agreement with Eq. (3). This value can be obtained also from the energy shift between the ion energy distributions of the first ionized atoms group and of the second ionized one. The results also demonstrated that the equivalent acceleration voltage increases with the free electron density of the irradiated metals, as reported in Figure 5b.

The relative amount of the first ionized atoms with respect to the neutral one grows with the electron density of the irradiated target, as reported in Figure 6a. The high value of the ratio indicates a substantial predominance of the first ionized atoms with respect to the neutrals in the direction of the normal to the target surface. However, previous measurements of angular distributions indicated that the neutrals have a larger angular distribution with respect to the ions and that their total amount can be comparable or higher (specially near the ablation threshold) with respect to the first ionized atoms contribution (Hansen *et al.*, 1997). The relative amount of the first ionized atoms with respect to
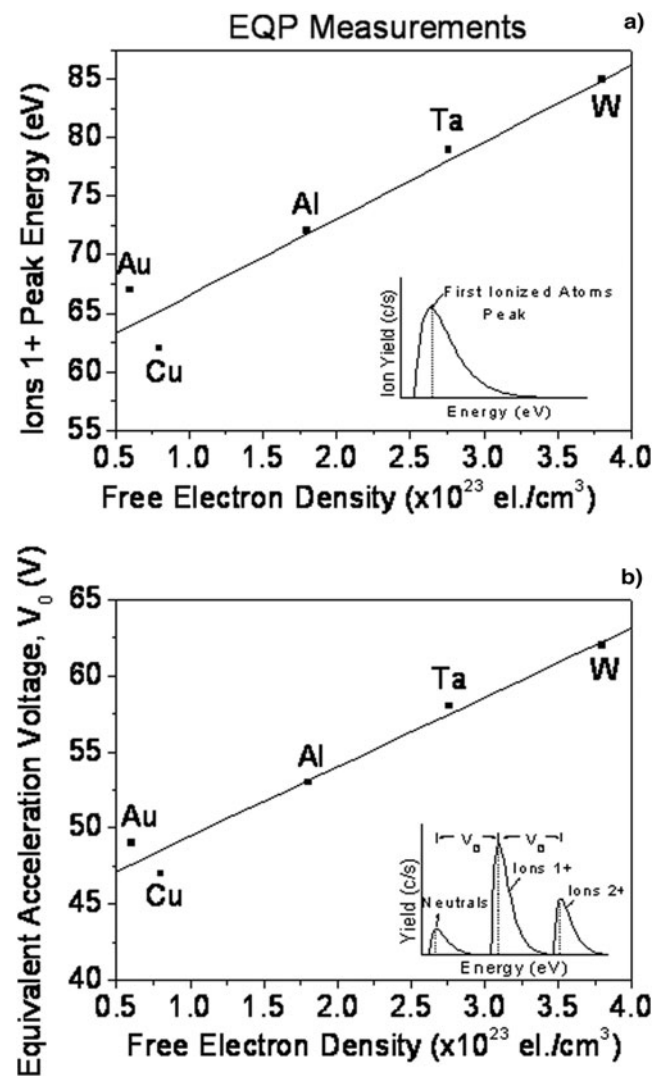
the second ionized ones decreases with the free electron density of the irradiated target, as reported in Figure 6b. This ratio refers to two ionic species having, approximately, the same angular distribution (it decreases slowly with the charge state) but a different ionization cross-section (it decreases quickly with the charge state) (Shirkov & Zschornak, 1996).

Preliminary results obtained with EQP indicate that the maximum charge state for the five ablated elements obtainable at 25 mJ pulse energy is 2+ for Cu, Al, and Au, and 3+ for Ta and W. This result is in good agreement with the ionization potential values of the elements (Zschornak *et al.*, 1986). In fact, assuming an average plasma temperature of about 8 eV, the mean thermal electron energy is about 12 eV. Because the energy distribution has a tail up to about three times than the mean energy, this means that electrons with energies of about 36 eV are present in the plasma. At this energy level the expected ionizations are
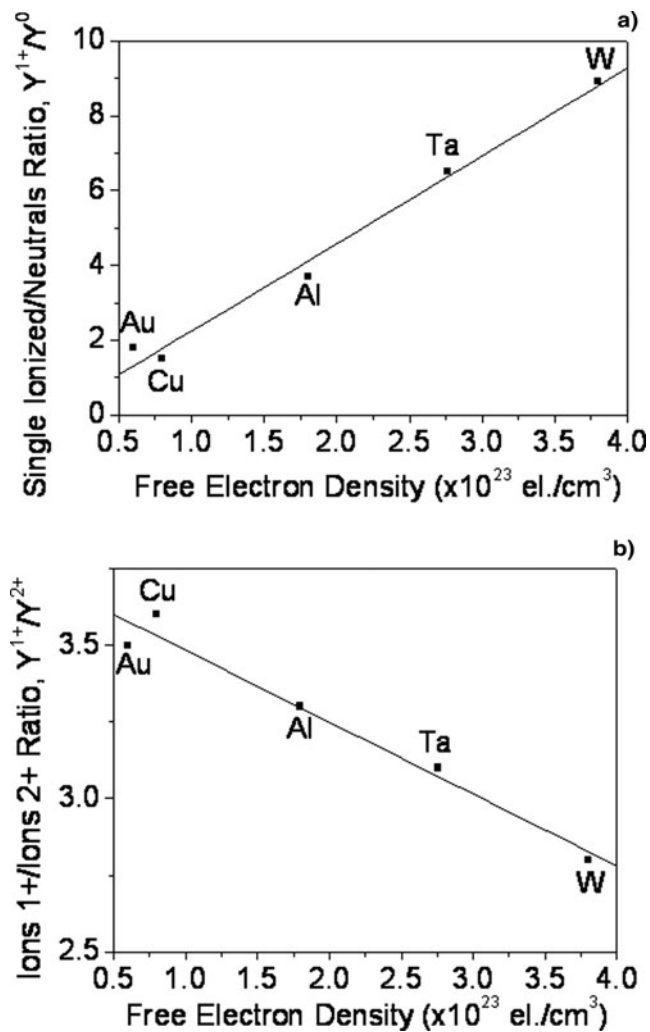
**Fig. 6.** The relative amount of the first ionized atoms with respect to the neutral one (**a**) and that of the first ionized with respect to the second ionized ones (**b**) as a function of the free electron density of the irradiated targets.

**Fig. 7.** The ionization potentials as a function of the charge states for the ablated targets.

2+ for Cu, Au, and Si, and 3+ for Ta and W, as reported in Figure 7.

Table 1 resumes the main parameters characterizing the five laser generated plasmas: the free electron density, the ablation threshold (obtained from Torrisi *et al.* (2007)), the ablation yield, the measured kinetic energies of the neutrals, first and second ionized atoms, the measured single ionized/neutrals and single ionized/double ionized ratios, the equivalent ion acceleration voltage, and the plasma temperature extrapolated from the experimental fit data.

## CONCLUSIONS

Experimental results obtained with EQP detector permitted us to determine directly the plasma temperature fitting the energy distributions of the neutral and ionic species. Moreover, the Coulomb-Boltzmann-shifted function, written in terms of kinetic energy, permitted us to evaluate
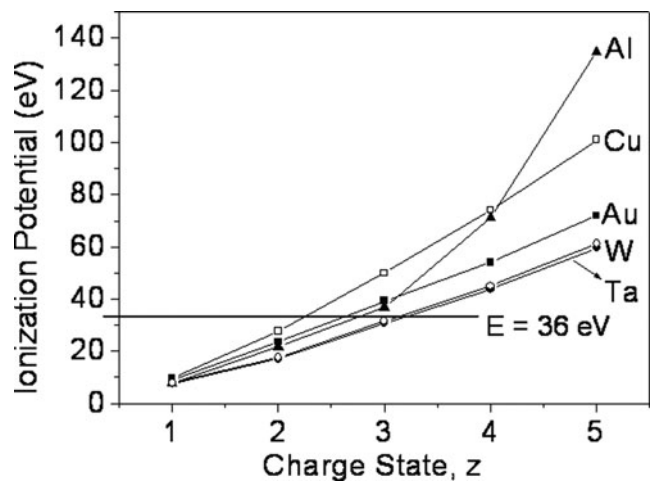
the equivalent ion acceleration voltage developed inside the laser-generated plasma and due to the non-equilibrium (in space and in time) of the charge distribution in the plasma, in agreement with literature (Torrisi *et al.*, 2006).

Although elements with high evaporation point, as W for example, need more energy to evaporate in vacuum and, consequently, a lower laser pulse energy is available to generate the plasma, measurements demonstrated that in this case, the mean energy of the neutral specie is higher with respect to that of elements with lower evaporation point. This means that the evaporation point, also being an important parameter, it is not sufficient to characterize the laser-produced plasma.

A possible explanation can be found in the lower density of the plasma, in the case of high evaporation temperature materials. On the contrary, laser ablation of low evaporation temperature materials produces higher dense vapor and the mean energy transferred to atoms and ions is lower with respect to the previous case, as for Al for example.

Experimental results indicate that the ablation yield is linearly dependent on the dc electrical conductivity of the irradiated element but it doesn't increase with the free electron density of the ablated target, probably due to the ablation process correlation with the heating conductivity of the material and not to its electronic configuration.

However, another important physical parameter, which strongly influences the plasma properties, is the plasma electron density that assumes an important role in the inverse bremsstrahlung absorption mechanism. This parameter is directly linked to the free electron density of the element constituting the ablated target, i.e., to the electron configuration of the elements. Results, in fact, demonstrate that the plasma temperature, the equivalent ion acceleration voltage, the ratio between the yields of ions 1+, and neutrals increase with the free electron density of the ablated element. The yield ratio between ions 1+ and 2+, instead, decreases with the free electron density, due to the increment of the second ionization yield with the plasma temperature. For these reasons

the free electron density of the metals can be considered as a key parameter for the non equilibrium plasma generated by visible pulsed lasers.

## REFERENCES

Bashir, S., Rafique, M.S. & Ul-Haq, F. (2007). Laser ablation of ion irradiated CR-39. *Laser Part. Beams* **25**, 181–191.

Batani, D., Dezulian, R., Redaelli, R., Benocci, R., Stabile, H., Canova, F., Desai, T., Lucchini, G., Krousky, E., Masek, K., Pfeifer, M., Skala, J., Dudzak, R., Rus, B., Ullschmied, J., Malka, V., Faure, J., Koenig, M., Limpouch, J., Nazarov, W., Pepler, D., Nagai, K., Norimatsu, T. & Nishimura, H. (2007). Recent experiments on the hydrodynamics of laser-produced plasmas conducted at the PALS laboratory. *Laser Part. Beams* **25**, 127–141.

Conde, J.C., Lusquinos, F., Gonzalez, P., Serra, J., Leon, B., Cultrera, L., Guido, D. & Perrone, A. (2004). Laser ablation of silicon and copper targets. Experimental and finite elements studies. *Appl. Phys. A.* **79**, 1105–1110.

Cranes Software Website (2006). http://www.cranesoftware.com/products/systat.

Fernandez, J.C., Hegelich, B.M., Cobble, J.A., Flippo, K.A., Letzring, S.A., Johnson, R.P., Gautier, D.C., Shimada, T., Kyrala, G.A., Wang, Y.Q,. Wetteland, C.J. & Schreiber, J. (2005). Laser-ablation treatment of short-pulse laser targets: Toward an experimental program on energetic-ion interactions with dense plasmas. *Laser Part. Beams* **23**, 267–273.

Hansen, T.N., Schou, J. & Lunney, J.G. (1997). Angular distributions of silver ions and neutrals emitted in vacuum by laser ablation. *Europhys. Lett* **40**, 441–446.

Hiden Analytical Website (2006). http://www.hidenanalytical.com/products.

Jungwirth, K. (2005). Recent highlights of the PALS research program. *Laser Part. Beams* **23**, 177–182.

Laska, L., Badziak, J., Boody, F.P., Gammino, S., Jungwirth, K., Krasa, J., Krousky, E., Parys, P., Pfeifer, M., Rohlena, K., Ryc, L., Skala, J., Torrisi, L., Ullschmied, J. & Wolowski, J. (2007). Factors influencing parameters of laser ion sources. *Laser Part. Beams* **25**, 199–205.

Lorazo, P., Lewis, L.J. & Meunier, M. (2006). Thermodynamic pathways to melting, ablation, and solidification in absorbing solids under pulsed laser irradiation. *Phys. Rev. B* **73**, xxx–xxx.

Nelea, V., Morosanu, C., Iliescu, M. & Mihailescu, I.N. (2004). Hydroxyapatite thin films grown by pulsed laser deposition and radio-frequency magnetron sputtering: comparative study. *Appl. Surf. Sci.* **228**, 346–356.

Schaumann, G., Schollmeier, M.S., Rodriguez-Prieto, G., Blazevic, A., Brambrink, E., Geissel, M., Korostiy, S., Pirzadeh, P., Roth, M., Rosmej, F.B., Faenov, A.Y., Pikuz, T.A., Tsigutkin, K., Maron, Y., Tahir, N.A. & Hoffmann, D.H.H. (2005). High energy heavy ion jets emerging from laser plasma generated by long pulse laser beams from the NHELIX laser system at GSI. *Laser Part. Beams* **23**, 503–512.

Shirkov, G.D. & Zschornak, G. (1996). *Electron Impact Ion Sources for Charged Heavy Ions*. Vieweg, Unknown City.

Thareja, R.K. & Sharma, A.K. (2006). Reactive pulsed laser ablation: Plasma studies. *Laser Part. Beams* **24**, 311–320.

Torrisi, L., Borrielli, A. & Margarone, D. (2007). Study on the ablation threshold induced by pulsed lasers at different wavelengths. *Nucl. Instr. & Meth. Phys. Res. Section B* **255**, 373–379.

Torrisi, L., Caridi, F., Margarone, D., Picciotto, A., Mangione, A. & Beltrano, J.J. (2006). Carbon-plasma produced in vacuum by 532 nm-3 ns laser pulses ablation. *Appl. Surf. Sci.* **252**, 6383–6389.

Torrisi, L., Caridi, F., Picciotto, A., Margarone, D. & Borrielli, A. (2006). Particle emission from tantalum plasma produced by 532 nm laser pulse ablation. *Appl. Phys.* **100**, 9.

Torrisi, L., Gammino, S., Ando, L. & Laska, L. (2002). Tantalum ions produced by 1064 nm pulsed laser irradiation. *J. Appl. Phys* **91**, 4685–4692.

Torrisi, L., Gammino, S., Ando, L., Nassisi, V., Doria, D. & Pedone, A. (2003). Comparison of nanosecond laser ablation at 1064 and 308 nm wavelength. *Appl. Surf. Sci.* **210**, 262–273.

Veiko, V.P., Shakhno, E.A., Smirnov, V.N., Miaskovski, A.M. & Nikishin, G.D. (2006). Laser-induced film deposition by LIFT: Physical mechanisms and applications. *Laser Part. Beams* **24**, 203–209.

Wieger, V., Strassl, M. & Wintner, E. (2006). Pico- and micro-second laser ablation of dental restorative materials. *Laser Part. Beams* **24**, 41–45.

Wolowski, J., Badziak, J., Czarnecka, A., Parys, P., Pisarek, M., Rosinski, M., Turan, R. & Yerci, S. (2007). Application of pulsed laser deposition and laser-induced ion implantation for formation of semiconductor nano-crystallites. *Laser Part. Beams* **25**, 65–69.

Zschornak, G., Musiol, G. & Wagner, W. (1986). *Dirac-Fock Slater X-ray Energy Shifts and Electron Binding Energy Changes for All Ion Ground States in Elements up to Uranium*, pp. 160–255. Berlin: Akademie der Wissenschaften der DDR.